

See discussions, stats, and author profiles for this publication at: <https://www.researchgate.net/publication/261506802>

# Weak C–H···O and Dipole–Dipole Interactions as Driving Forces in Crystals of Fluorosubstituted Phenylboronic Catechol Esters

ARTICLE in CRYSTAL GROWTH & DESIGN · NOVEMBER 2013

Impact Factor: 4.89 · DOI: 10.1021/cg4012026

---

CITATIONS

11

READS

50

## 6 AUTHORS, INCLUDING:



Michał Jakubczyk

Lodz University of Technology

8 PUBLICATIONS 62 CITATIONS

[SEE PROFILE](#)



Izabela Madura

Warsaw University of Technology

42 PUBLICATIONS 250 CITATIONS

[SEE PROFILE](#)



Agnieszka Adamczyk-Woźniak

Warsaw University of Technology

34 PUBLICATIONS 247 CITATIONS

[SEE PROFILE](#)



Alicja Matuszewska (Pawełko)

Warsaw University of Technology

9 PUBLICATIONS 50 CITATIONS

[SEE PROFILE](#)

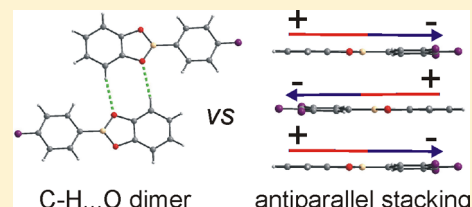
# Weak C–H…O and Dipole–Dipole Interactions as Driving Forces in Crystals of Fluorosubstituted Phenylboronic Catechol Esters

Izabela D. Madura,\* Karolina Czerwińska, Michał Jakubczyk, Alicja Pawelko, Agnieszka Adamczyk-Woźniak, and Andrzej Sporzyński

Warsaw University of Technology, Faculty of Chemistry, Noakowskiego 3, 00-664 Warsaw, Poland

## S Supporting Information

**ABSTRACT:** The analysis of weak interactions in crystals of a series of fluorosubstituted phenylboronic catechol esters (fphb) supported by Hirshfeld surface analysis is presented. The influence of the number and positions of fluorine atoms on the molecular structure is discussed and compared with results of the DFT calculations for isolated molecules. The molecular symmetry breaking caused by the intermolecular interactions was detected. The substantial differentiation of the dipole moments generated by fluorine substitution and its consequence on molecular packing are analyzed. The presence of *ortho*-fluoro substituents was found to enhance the proton acceptor character of oxygen atoms. Consequently, the C–H…O hydrogen-bonded centrosymmetric dimer is the dominating motif for molecules with small dipole moments. Otherwise, the antiparallel dipole–dipole interactions are responsible for the supramolecular architecture.



## INTRODUCTION

Noncovalent weak intermolecular interactions have gained much attention due to their unquestionable role in various chemical, physical, and biological processes.<sup>1</sup> Their influence on molecular aggregation is still a subject of discussions basing on experimental and theoretical techniques.<sup>2,3</sup> Among these interactions, excluding ionic effects, the hydrogen bonds are the most important in view of their energy and directionality.<sup>4,5</sup> Also, the hydrogen bonds formed by C–H donors are nowadays well-established in the crystallographers community<sup>6–10</sup> as well as they are under investigation of theoreticians.<sup>11–13</sup> Moreover, there are miscellaneous weaker interactions, which are also important, particularly in the absence of hydrogen bonds.<sup>14,15</sup> Since the molecules of esters examined here contain aromatic rings as well as fluorine substituents and a boronic BO<sub>2</sub> moiety, particular attention is paid in this article to weak C–H…A (A = O or F) hydrogen bonds and aromatic interactions.

Starting from the late 90s of the previous century, the C–H…O interactions are regarded as weak, but significant, directional intermolecular forces with the energy estimated around 1–2 kcal/mol.<sup>6,7</sup> Moreover, recent papers show that these interactions are able to mimic the stronger classical H-bonds (e.g., forming a helical structure<sup>16</sup>) or even to compete with them.<sup>17</sup>

As far as C–H…F hydrogen bonds are concerned, they are said to be at the borderline of the hydrogen bond phenomenon and show poor directionality.<sup>8,13</sup> The cause of this is seen in the hardness of the F atom,<sup>18</sup> which, according to Pearson's theory,<sup>19</sup> is connected with its poor hydrogen bond acceptor properties despite the high electronegativity difference between carbon and fluorine. Nevertheless, recent studies clearly show that, in the absence of other meaningful interactions, the C–

H…F hydrogen bonds can play a role in the overall crystal packing of molecules.<sup>8,9</sup> Moreover, their utility in crystal engineering through the well-recognized synthons is also documented.<sup>8</sup> It should be noticed that an important issue concerning hydrogen bonds is their cooperativity.<sup>6,11</sup> When there are arrays of interconnected hydrogen bonds, the donors and acceptors increase their polarization mutually, thereby strengthening the individual bonds. The energy enhancement due to cooperativity may attain values over 20%.

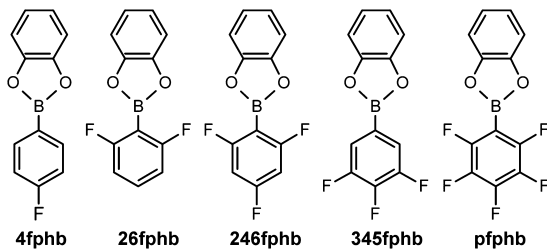
The aromatic rings' interactions are usually considered in four prototypical systems of the benzene dimer: parallel-displaced, eclipsed face-to-face (sandwich), T-shaped, and edge-to-face. The last two modes are more aptly described as aromatic C–H…π interactions.<sup>10</sup> They are regarded as weak hydrogen bonds occurring between soft acids and soft bases. The crystal structure of benzene is the best reference confirming the significance of these interactions.<sup>20</sup> Further, the parallel-displaced and eclipsed face-to-face modes are nowadays studied in respect to substituent effects in aromatic systems.<sup>14,21</sup> Among them, the interactions between arene and perfluoroarene molecules (or containing both fragments in one molecule<sup>22</sup>) are of great interest.<sup>14,23</sup> Because of these interactions, the parallel stacking of alternating perfluoroarene and arene rings resulting in a columnar arrangement was observed. It was estimated that these stacking interactions feature a stabilizing energy of about 7 kcal/mol.<sup>14</sup>

The presented study concerns the crystal structure analysis of five fluorophenylboronic catechol esters (Scheme 1). When it comes to the discussion on possible intermolecular interactions,

Received: August 7, 2013

Revised: October 17, 2013

Published: October 29, 2013

**Scheme 1**

there is another aspect to be taken into account. Because of the fact that a boron center is present in the studied esters, they are able to create adducts with electron pair donors. It should be mentioned that the Lewis acidity of catechol esters is reasonably high, and higher than for other esters and comparable to that of triarylboranes.<sup>24,25</sup> These properties provide ample opportunities in the crystal engineering field, as it was shown by Yaghi et al.<sup>26</sup> as well as in Suzuki coupling reactions,<sup>27</sup> sugar<sup>28</sup> and fluoride<sup>29</sup> sensing, or polymer electrolyte additives.<sup>24</sup> Last, but not least, short contacts with boron atoms may also be found in crystals of boronic esters influencing the molecular organization.<sup>30–32</sup>

## EXPERIMENTAL SECTION

**Synthesis and Crystallization.** A series of fluorophenylboronic catechol esters have been synthesized according to the procedure given by Adamczyk-Woźniak et al.<sup>24</sup> Single crystals appropriate for X-ray diffraction measurements were obtained by crystallization from the following solvents: 4-fluorophenylboronic (**4fphb**) and 3,4,5-trifluorophenylboronic derivatives (**345fphb**) from methyl alcohol with chloroform, 2,6-difluorophenylboronic (**26fphb**) from chloroform, and 2,4,6-trifluorophenylboronic (**246fphb**) from hexane. High-quality single crystals of pentafluorophenylboronic catechol ester (**pfphb**) were obtained by sublimation.

**X-ray Crystallographic Studies.** Crystal data for all esters, data collection, and details of refinement are given in Table 1. The single-crystal X-ray experiments were conducted on the Gemini A Ultra Diffractometer (Agilent Technologies) equipped with a CCD detector, using mirror monochromated Cu radiation ( $\lambda = 1.5418 \text{ \AA}$ ). All crystals were measured at 100(2) K in a stream of cold nitrogen. Data collection and data reduction were performed in the CrysAlis<sup>Pro</sup> program.<sup>33</sup> To solve and refine the structures, the OLEX-2 suite<sup>34</sup> with implemented SHELXS97 (direct methods) and SHELXL97 (the full-matrix least-squares technique) programs<sup>35</sup> was used. All non-hydrogen atoms were refined with anisotropic temperature factors.

The hydrogen atoms were placed in calculated positions with fixed isotropic thermal parameters ( $U_{\text{iso}}(\text{H}) = 1.2 \times [U_{\text{eq}}(\text{C})]$ ) and were included in the structure factor calculations in the final stage of the refinement. Values involving hydrogen atoms in the calculated positions are given without estimated standard deviations. In the case of the **345fphb** structure, the Flack parameter ( $x$ )<sup>36</sup> has refined to the value of 0.3(4), indicating the presence of the inversion twin. Attempts to refine the structure in the suitable centrosymmetric *Pbca* space group gave higher refinement factors and nonphysical thermal parameters. For the analysis of bond lengths, bond angles, and other geometrical parameters, the PLATON program<sup>37</sup> was applied. Molecular and packing diagrams were generated using DIAMOND<sup>38</sup> and ORTEP-3 for Windows.<sup>39</sup>

**Computational Details.** All geometries of the esters were prepared manually and submitted for full optimization without any symmetry restraints at the RB3LYP/6-311G(2df,p) level of theory. Frequencies were calculated to ensure that the optimized structure is not a transition state (see Table S3 in the Supporting Information). All computations were carried out using the Gaussian 09<sup>40</sup> quantum chemistry package. The presented molecular electrostatic potential (ESP) layouts are mapped on the electron density isosurface  $\rho(r) = 0.004 \text{ e \AA}^{-3}$ . The ESP at a given point near a molecule is a measure of the electrostatic energy a positive unit test charge would have at that point. Negative ESPs correspond to an attractive interaction with the test charge, whereas positive ESPs indicate repulsion. The HOMO–LUMO orbitals have been rendered from Gaussian 09 formatted checkpoint files. The isosurface value is equal to 0.0355.

**Hirshfeld Surface Analysis.** The molecular Hirshfeld surfaces (HS)<sup>41</sup> and their associated 2D-fingerprint plots<sup>42</sup> were calculated from crystal structure coordinates using the CrystalExplorer program.<sup>43</sup> The surfaces are constructed based on the electron distribution calculated as the sum of spherical atom electron densities. For each point on the surface, the distances to the closest atom inside and outside the surface are measured and defined as the  $d_i$  and  $d_e$  parameters, respectively.<sup>41</sup> The normalized contact distance ( $d_{\text{norm}}$ ) based on both  $d_e$  and  $d_i$  and the vdW radii ( $r$ ) of atoms is given by the equation,  $d_{\text{norm}} = [(d_i - r_i)/r_i] + [(d_e - r_e)/r_e]$ . In Figure 4, the HS are mapped with  $d_{\text{norm}}$  over the range of −0.8 to 1.2 Å with the red–white–blue coloring scheme (red, shorter than the sum of van der Waals radii, through white to blue, greater than the sum of radii). The van der Waals radii were chosen to be equal to those used in CSD.<sup>44</sup> The 2D-fingerprint plots were derived from the HS by plotting the fraction of points on the surface as a function of the pair ( $d_i, d_e$ ). Each point on the 2D graph represents a bin formed by discrete intervals of  $d_i$  and  $d_e$  (0.01 Å × 0.01 Å), and the points are colored as a function of the fraction of surface points in that bin, with a range from blue (relatively few points) through green (moderate fraction) to red (highest fraction). The range of fractions spanning 0.05% of surface areas was used. The full fingerprint plots are presented in Figure S1

**Table 1. Crystallographic Parameters for the Crystal Structures of Studied Esters**

compound	<b>4fphb</b>	<b>26fphb</b>	<b>246fphb</b>	<b>345fphb</b>	<b>pfphb</b>
formula	C <sub>12</sub> H <sub>8</sub> BF <sub>2</sub> O <sub>2</sub>	C <sub>12</sub> H <sub>7</sub> BF <sub>2</sub> O <sub>2</sub>	C <sub>12</sub> H <sub>6</sub> BF <sub>3</sub> O <sub>2</sub>	C <sub>12</sub> H <sub>6</sub> BF <sub>3</sub> O <sub>2</sub>	C <sub>12</sub> H <sub>4</sub> BF <sub>5</sub> O <sub>2</sub>
m. wt.	213.99	231.99	249.98	249.98	285.96
T (K)	100.0(2)	100.0(2)	100.0(2)	100.0(2)	100.0(2)
system	monoclinic	monoclinic	monoclinic	orthorhombic	monoclinic
space group	<i>P</i> 2 <sub>1</sub> / <i>n</i>	<i>P</i> 2 <sub>1</sub> / <i>n</i>	<i>P</i> 2 <sub>1</sub> / <i>n</i>	<i>P</i> 2 <sub>1</sub> 2 <sub>1</sub> 2 <sub>1</sub>	<i>P</i> 2 <sub>1</sub> / <i>n</i>
<i>a</i> (Å)	12.3005(7)	4.70657(10)	4.6638(4)	6.81454(18)	7.4212(2)
<i>b</i> (Å)	4.7059(3)	16.2704(3)	16.2633(9)	11.5913(3)	6.08906(17)
<i>c</i> (Å)	17.2280(9)	12.9604(2)	13.3246(8)	13.0881(4)	23.4084(6)
$\beta$ (deg)	98.363(5)	97.9090(19)	97.377(6)	90	92.321(3)
vol. (Å <sup>3</sup> )	986.63(9)	983.04(3)	1002.28(12)	1033.82(5)	1056.91(5)
<i>Z</i>	4	4	4	4	4
<i>D</i> <sub>calc</sub> (mg/m <sup>3</sup> )	1.441	1.567	1.657	1.606	1.797
<i>R</i> <sub>1</sub> ( <i>I</i> > 2 <i>σ</i> ( <i>I</i> ))	0.0444	0.0300	0.0288	0.0258	0.0299
<i>wR</i> <sub>2</sub> (on <i>F</i> <sup>2</sup> , all data)	0.1222	0.0825	0.0786	0.0702	0.0773

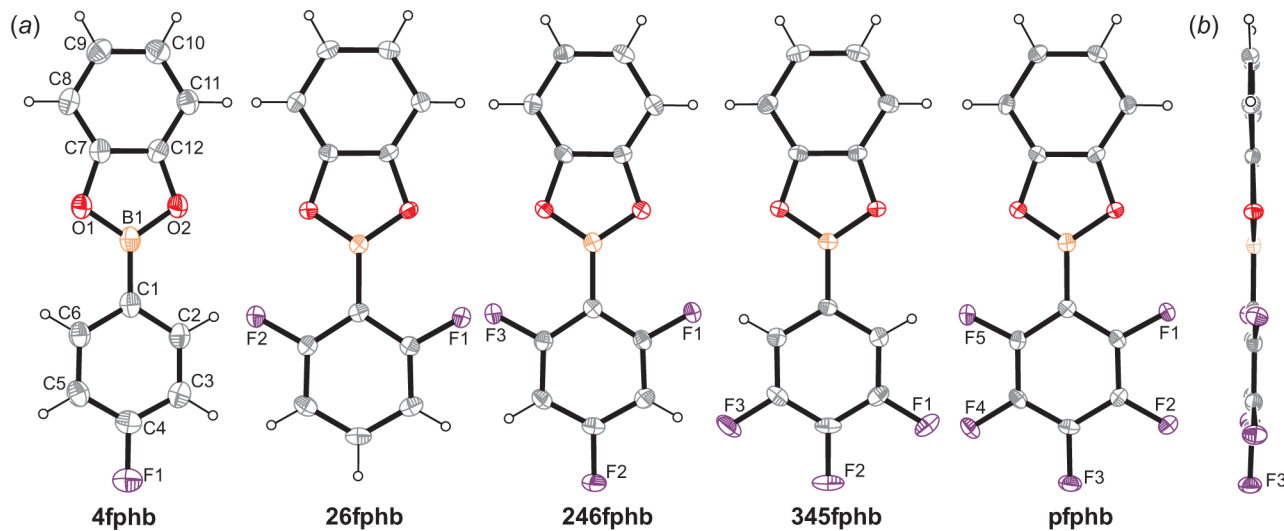


**Figure 1.** ORTEP<sup>39</sup> drawings of the ester molecules. The ellipsoids are shown at 50% probability. (a) A numbering scheme of common heavy atoms is shown on the **4fphb** molecule while a numbering of fluorine atoms is given for all molecules. (b) Side view of the **pfphb** molecule.

**Table 2. Selected Geometrical Parameters for Molecules in Crystals and for Molecules Optimized at the Density Functional Theory RB3LYP/6-311G(2df,p) Level (*Italic*) (Å, deg), Continuous Symmetry Measure Parameter (CSM), Melting Points (m.p. in °C), Dipole Moments (from DFT) ( $\mu$  in D), and Energy of HOMO–LUMO Gap (from DFT) (eV)**

	<b>phb<sup>a</sup></b>	<b>4fphb</b>	<b>26fphb</b>	<b>246fphb</b>	<b>345fphb</b>	<b>pfphb</b>
B–C1	1.537(2) 1.539	1.533(3) 1.538	1.553(2) 1.549	1.553(2) 1.547	1.546(2) 1.542	1.558(2) 1.552
B–O1	1.394(2)	1.394(2)	1.386(2)	1.384(2)	1.383(2)	1.383(2)
B–O2	1.394(2) 1.391	1.394(2) 1.391	1.385(2) 1.387	1.381(2) 1.387	1.379(2) 1.387	1.380(2) 1.384
O–B–O	109.8(1) 110.6	111.0(1) 110.7	111.7(1) 110.8	112.1(1) 110.9	112.2(1) 111.1	112.4(1) 111.2
O1–B–C1	125.1(1)	124.0(1)	123.9(1)	124.3(1)	123.8(1)	124.3(1)
O2–B–C1	125.1(1) 124.7	125.1(1) 124.6	124.4(1) 124.6	123.6(1) 124.6	124.0(1) 124.5	123.3(1) 124.4
CSM	0.07(3)	0.10(3)	0.17(4)	0.04(2)	0.27(5)	0.17(4)
m.p.	110	96	123	130	140	137
$\mu$	0.02	-1.37	0.93	-0.45	-3.12	-2.18
energy gap	5.14	5.18	4.92	4.99	5.01	4.83

<sup>a</sup>Values extracted from the CIF file deposited in CSD<sup>44</sup> under refcode PBXBOR and associated with ref 47. The numbering scheme was changed to be in accordance with the one used here.

(Supporting Information) while these resolved for highlighted contacts in Figure 5, Figure 6 (selected), and Figure S2 of the Supporting Information (all). For the decomposed fingerprint plots presenting particular contacts, the outline of the full fingerprint is shown in gray.

## RESULTS AND DISCUSSION

The analysis of five crystal structures of a series of fluorosubstituted phenylboronic catechol esters is presented. The molecules in crystals of studied esters are presented in Figure 1. It should be mentioned that the structures of pentafluorophenylboronic catechol ester (**pfphb**)<sup>45</sup> as well as 4-fluorophenylboronic catechol ester (**4fphb**)<sup>46</sup> were already published, but the data were measured at 296 and 200 K, respectively, and no detailed discussion of their crystal structure was given. Hence, the analysis of their structures determined at 100 K is presented here. It should be underlined that lowering of the temperature has not affected significantly the crystal structures in both cases. Relevant crystallographic data and selected geometric parameters for presented esters are given in Tables 1 and 2, respectively. The full geometrical information is

summarized in Tables S1 and S2 of the Supporting Information.

**Molecular Structures.** Compounds **4fphb**, **26fphb**, **246fphb**, and **pfphb** crystallize in the centrosymmetric  $P_{2_1}/n$  space group of the monoclinic system, whereas **345fphb** crystallizes in a chiral  $P_{2_1}2_12_1$  space group symmetry of the orthorhombic system. In all cases, there is only one molecule in the asymmetric unit (Figure 1). They are not located on any crystallographic symmetry element, in contrast to the molecules of the unsubstituted phenylboronic catechol ester (**phb**)<sup>47</sup>, which possesses crystallographic  $C_s$  symmetry. The quantitative measure of the deviation from the assumed molecular symmetry is well-reflected by the Continuous Symmetry Measure parameter (CSM) proposed by Zabrodsky et al.<sup>48</sup> All studied molecules together with **phb** seem to have the symmetry close to the  $mm2$  ( $C_{2v}$ ) point group. The CSM parameter (Table 2), which increases with the deviation from the exact point group symmetry, varies for the considered molecules from 0.04(3) for **246fphb** to 0.27(5) for **345fphb**. It is important to note that the geometry of all the ester molecules

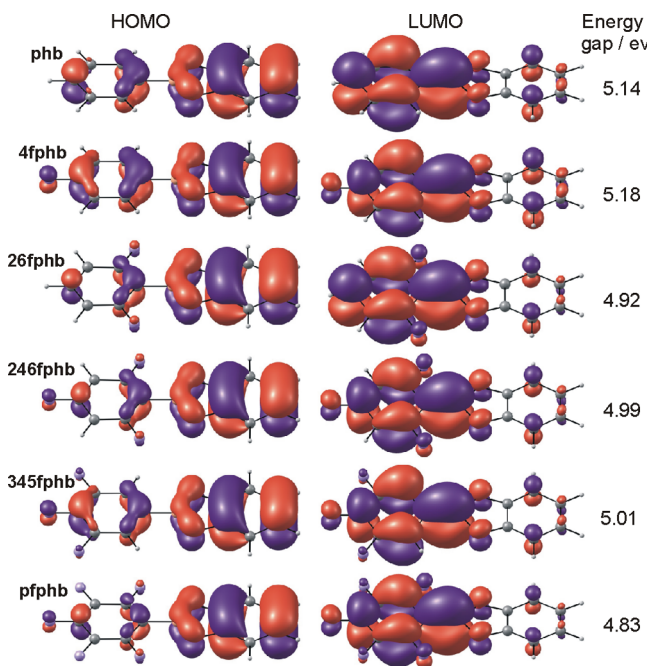


Figure 2. HOMO and LUMO molecular orbitals for ester molecules optimized at the DFT theory RB3LYP/6-311G(2df,p) level.

(see Tables S1 and S2 in the Supporting Information) optimized by the DFT method is exactly the  $C_{2v}$ . This indicates that the symmetry breaking may be induced by intermolecular interactions.

The discrepancy in the bond lengths is insignificant except for the B1–C1 bond elongation upon fluorine substitution. The analysis of bond angles values also does not give a clear answer about the impact of fluorine atoms on the molecular structure. In all the fluorinated derivatives, the boron center shows a trigonal coordination with the sum of bond angles close to  $360^\circ$ . The O1–B1–O2 angle is the smallest, and it is rising from  $109.8(2)^\circ$  to  $112.4(1)^\circ$  for **phb** and **pfphb**, respectively. In the case of isolated molecules, the tendency is the same but the difference is less than  $1^\circ$  (Table 2). Generally, the optimized geometries and those found in the crystals are very akin. For example, in all cases, the catechol ring's angles C7–C8–C9 and C10–C11–C12 are narrowed comparing to unbound catechol molecules<sup>49</sup> and reach the value of  $\sim 116^\circ$ . This can be explained by the strains caused by the formation of the  $BO_2C_2$  five-membered ring. Nevertheless, the differences in geometry of studied molecules turned out to be very subtle, which results from the compensation of inductive and resonance effects of the fluorine substituent.

This is also reflected when comparing the shape of the esters' HOMO–LUMO molecular orbitals (Figure 2). They look almost the same despite the increasing number of fluorine atoms. Further, only a small decrease by  $\sim 0.3$  eV in the energy of the HOMO–LUMO gap is observed when going from **phb** to **pfphb**. It is noteworthy that the HOMO orbitals are mainly located on the catechol fragment, indicating its donor character, whereas the LUMO orbitals appear over the boron atom and the phenyl ring. Therefore, this part of the molecule shows acceptor properties. Molecular electrostatic potential surface maps (ESP) are also helpful for the analysis of potential intermolecular donor and acceptor regions in molecules.<sup>14</sup> Figure 3 presents the ESP maps calculated for the DFT-optimized ester molecules.

The negative areas are associated with possible donor sites, i.e., ones willing to interact with the positive charge. They are located on the oxygen atoms, especially in the cases of di-*ortho*-fluoro derivatives **26fphb** and **246fphb**. The positive areas are found on boron and hydrogen atoms, indicating them as possible electron acceptors or hydrogen bond donors, respectively. On the ESPs, the influence of subsequent fluorination is mostly reflected in the change of the phenyl ring's sign when coming from the unsubstituted (**phb**) to pentafluoro derivative (**pfphb**). In the latter, as well as in **345fphb** one, the polarization between heads and tails of the molecules is consistent with the calculated dipole moment for DFT-optimized molecules (Table 2). In all cases, the dipole vector extends in accordance to the direction of the molecular 2-fold axis (i.e., through the B–C bond). It should be pointed here that, in the cases of derivatives without fluorine atoms at the *para* position (**phb** and **26fphb**), the orientation of the dipole vector is reversed; i.e., the negative pole is located on the catechol fragment while the positive one is on the phenyl ring. Summarizing, it is interesting whether the localization of HOMO–LUMO orbitals and the differentiation of the positive and negative regions on ESP maps with the associated dipole moments are reflected at the supramolecular level.

**Crystal Structure and Intermolecular Interactions.** As mentioned in the Introduction, the weak hydrogen bonds with C–H donors as well as the aromatic interactions and those involving boron atoms may be formed between the ester molecules in crystals. In the case of **phb**, the herringbone layers directed by C–H $\cdots\pi$  hydrogen bonds and the offset stacking were previously identified.<sup>47</sup> A similar molecular arrangement was also observed in the case of the structure of bis(dioxa-borole) catechol ester.<sup>50</sup> In this paper, geometrical considerations (Tables 3 and 4) are supported by the Hirshfeld surface analysis,<sup>41,42</sup> which is a very convenient tool for the elucidation of intermolecular contacts. Figure 4 presents front and back sides of the studied ester molecules in crystals. The

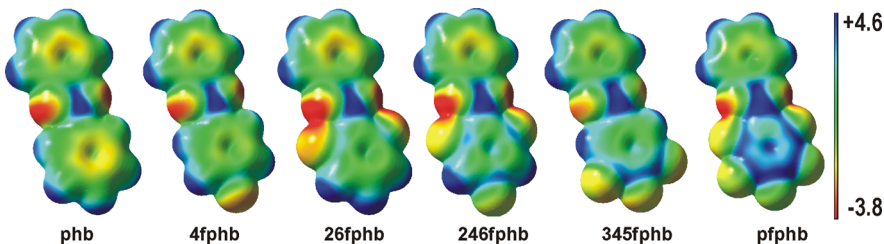


Figure 3. Calculated molecular electrostatic potential surfaces (ESP) mapped on the electron density isosurface  $\rho(r) = 0.004 \text{ e } \text{\AA}^{-3}$  for ester molecules optimized at the DFT theory RB3LYP/6-311G(2df,p) level.

Table 3. Geometry of Intermolecular Hydrogen Bonds (Å, deg)

compound	contact	H···A	D···A	D-H···A	symmetry
C–H···O in dimers					
4fphb	C11–H11···O2	2.48	3.396(2)	161	1 – x, 1 – y, 1 – z
26fphb	C11–H11···O2	2.58	3.527(2)	172	–x, 1 – y, –z
246fphb	C11–H11···O2	2.56	3.507(2)	171	–x, 1 – y, –z
pfpfb	C11–H11···O2	2.66	3.541(2)	157	–x, 1 – y, –z
other C–H···O					
4fphb	C6–H6···O1	2.61	3.278(2)	128	3/2 – x, –1/2 + y, 1/2 – z
26fphb	C3–H3···O1	2.76	3.350(2)	121	1/2 + x, 1/2 – y, –1/2 + z
246fphb	C3–H3···O1	2.73	3.430(2)	131	1/2 + x, 1/2 – y, –1/2 + z
345fphb	C9–H9···O2	2.76	3.507(2)	136	3/2 – x, 1 – y, 1/2 + z
	C9–H9···O1	2.80	3.493(2)	131	1 – x, –1/2 + y, 3/2 – z
C–H···F in dimers					
26fphb	C11–H11···F1	2.66	3.243(2)	121	–x, 1 – y, –z
	C10–H10···F1	2.64	3.255(2)	123	–x, 1 – y, –z
246fphb	C11–H11···F1	2.62	3.271(2)	126	–x, 1 – y, –z
	C10–H10···F1	2.73	3.303(2)	119	–x, 1 – y, –z
pfpfb	C11–H11···F1	2.63	3.218(2)	122	–x, 1 – y, –z
	C10–H10···F1	2.74	3.253(2)	116	–x, 1 – y, –z
other C–H···F					
4fphb	C10–H10···F1	2.55	3.426(2)	154	1/2 + x, 1/2 – y, 1/2 + z
26fphb	C10–H10···F2	2.65	3.458(2)	143	1/2 – x, 1/2 + y, 1/2 – z
246fphb	C3–H3···F3	2.63	3.431(2)	143	1/2 – x, 1/2 + y, 1/2 – z
345fphb	C2–H2···F2	2.50	3.306(2)	142	1 – x, –1/2 + y, 1/2 – z
	C10–H10···F3	2.66	3.296(2)	124	x, –1 + y, z
	C11–H11···F3	2.69	3.288(2)	122	x, –1 + y, z
	C6–H6···F1	2.64	3.320(2)	129	3/2 – x, 2 – y, 1/2 + z
pfpfb	C9–H9···F3	2.55	3.231(2)	130	–1/2 + x, 5/2 – y, –1/2 + z
	C8–H8···F4	2.59	3.452(2)	154	1 – x, 3 – y, –z

Table 4. Parameters Describing the Relative Orientation of Stacking Molecular Planes (Å, deg)

4fphb	26fphb	246fphb	pfpfb	345fphb
in C–H···O dimers				
<i>p</i>	0.73(1)	0.55(1)	0.44(1)	0.95(1)
in stacks				
<i>d</i>	3.37(1)	3.29(1)	3.29(1)	3.38(1), 3.31(1)
<i>off</i>	3.3(1)	3.8(1)	3.3(1)	2.1(1), 1.8(1)
angle between stacking columns				
<i>θ</i>	87.1(1)	88.7(1)	88.0(1)	47.1(1)
				67.1(1)

red spots are indicators of intermolecular contacts with distances below the sum of the van der Waals radii of interacting atoms.

The red spots indicated by green solid arrows in Figure 4 result from the centrosymmetric well-recognized  $R_2^2(8)$  dimeric synthon<sup>51</sup> formed by C–H···O hydrogen bonds (Figure 5a). The importance of these interactions is additionally confirmed by the relatively long whiskers appearing on H···O/O···H resolved fingerprint plots (example in Figure 5c and full collection in Figure S2 of the Supporting Information). This dimeric motif occurs in **4fphb**, **26fphb**, and **246fphb** derivatives. In **pfpfb**, the analogous dimeric synthon is also found, but the shift between molecules along the vector perpendicular to the molecule's plane (parameter *p* in Table 4, Figure 5b) of 0.95(1) Å slightly weakens these interactions in terms of geometrical parameters. In **246fphb**, the molecules in the dimer are nearly coplanar (*p* = 0.44(1) Å). Moreover, in all the *ortho*-substituted derivatives, this dimeric synthon is supported by bifurcated C–H···F interactions (Table 3). Consequently, two more motifs can be distinguished and

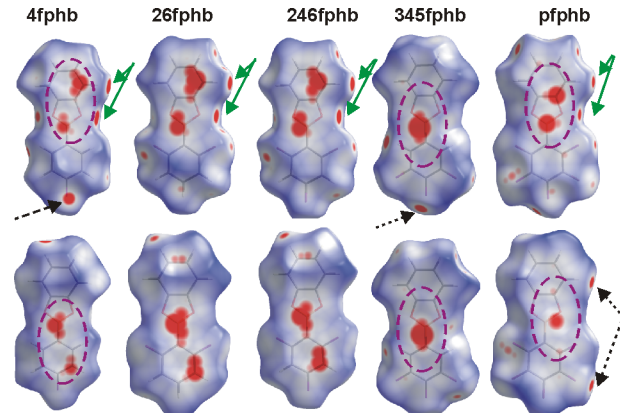
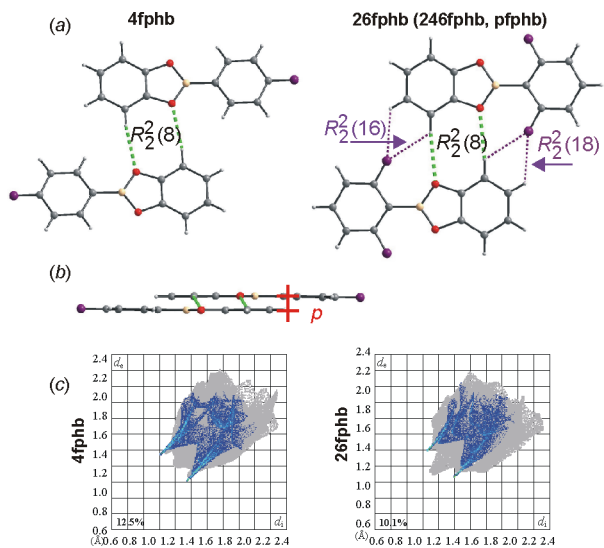


Figure 4. Molecular Hirshfeld surfaces mapped with  $d_{\text{norm}}$ . A red (contacts  $<$  vdW separations)—white (contacts  $\sim$  vdW separations)—blue (contacts  $>$  vdW separations) coloring scheme is used. Front and back sides of molecules are shown. Arrows point to the regions of C–H···O (solid green) and C–H···F (dotted black) hydrogen bonds while dashed purple circles indicate stacking interactions.

described by the  $R_2^2(18)$  and  $R_2^2(16)$  graph sets (Figure 5a). It is in accordance with the calculated ESP pattern (Figure 3) as well as with the cooperativity of hydrogen bonds. Such dimeric synthons are absent in crystals of the **345fphb** compound.

In all cases, there are intense red spots on Hirshfeld surfaces near the boron atom and the corresponding spots either on the catechol ring or on the phenyl ring. They are associated with the stacking interactions (Table 4) and appear in the 2D-fingerprint plots as areas at  $d_e + d_i$  around 3.6 Å (Figure S1, Supporting Information). It should be mentioned that, except



**Figure 5.** (a) Dimeric synthons directed by C–H...O hydrogen bonds. The appropriate graph descriptors<sup>51</sup> are given. (b) Side view of a dimer and definition of  $p$  parameter. (c) Examples of the H...O/O...H resolved 2D-fingerprint plots.

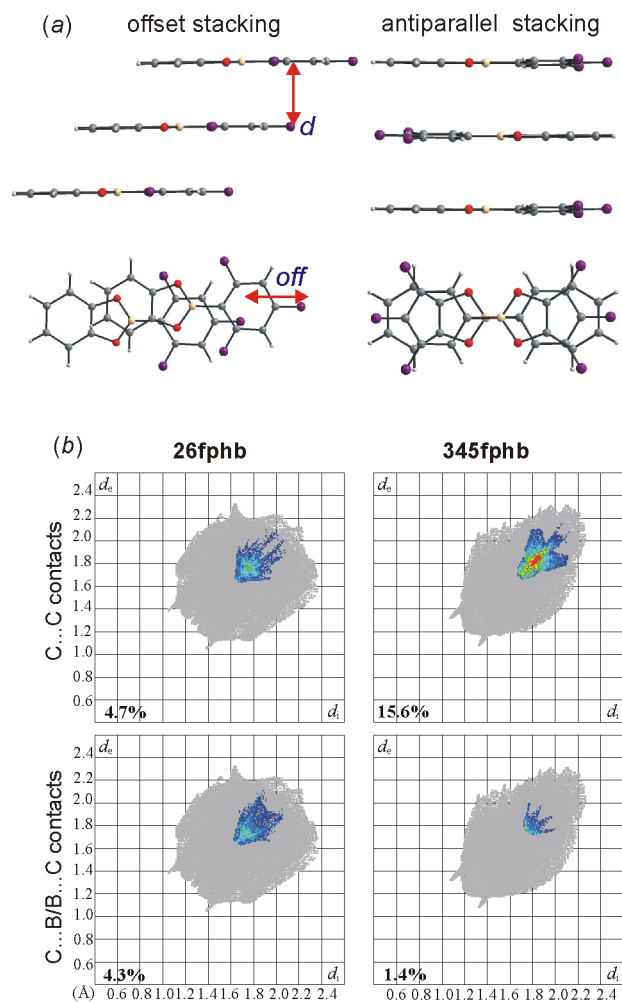


**Figure 6.** (a) Offset and antiparallel stacking synthons. (b) Example of C...C and B...C/C...B resolved 2D-fingerprint plots.

for the  $\pi\cdots\pi$  stacking interactions, the B... $\pi$  short contacts are also present. The analysis of the decomposed 2D-fingerprint

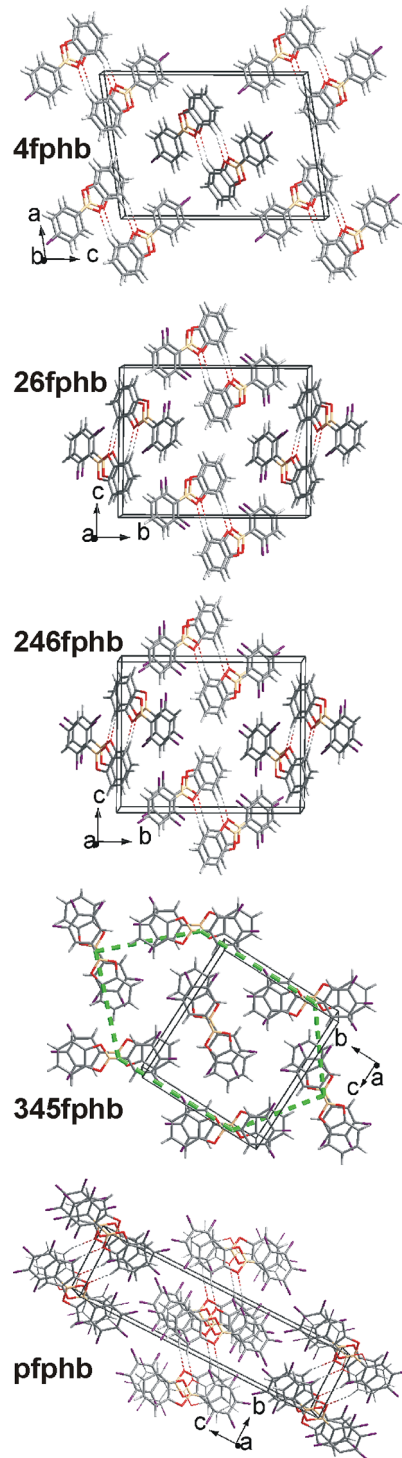


**Figure 7.** Packing diagrams for fluorosubstituted phenylboronic catechol esters. Thin dotted lines denote C–H...O hydrogen bonds. Thick green dotted lines indicate the close to hexagonal packing of molecular stacks in 345fphb.

plots (Figure S2, Supporting Information, and an example in Figure 6b) revealed that the characteristic “stacking” regions are associated with C...C and B...C contacts. Moreover, in the cases of the esters where the C–H...O dimeric motif is essential, the B...C and C...C resolved contacts are almost equally occupied at the level of ca. 5%. For 345fphb and pfphb, the surface coverage for C...C contacts is apparently higher and reaches ~15%, whereas the B...C/C...B contacts practically

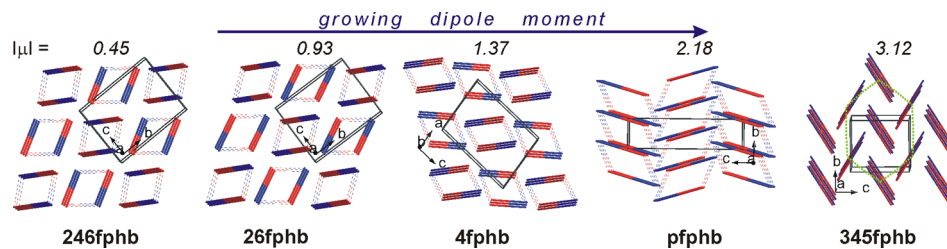


**Figure 8.** Simplified molecular packing showing the orientation of molecular dipoles. The molecules are reduced to a rod lying in accordance to the dipole moment vector position as well as the direction. The red and blue ends represent the positive and negative poles of the vector, respectively. The dotted lines stand for C–H...O hydrogen bonds. The values of dipole moments (in D) for optimized molecules at the DFT/RB3LYP/6-311G(2df,p) level in the gas phase are given. The green dotted lines indicate the close to hexagonal packing of stacks in **345fphb**.

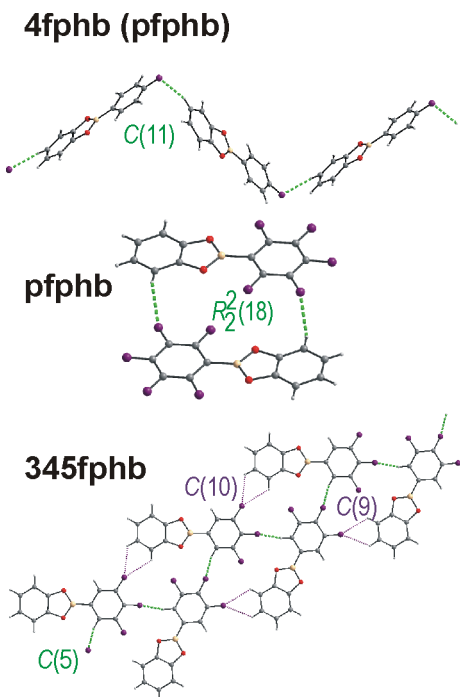


**Figure 9.** Supramolecular synthons directed by C–H...F interactions.

disappear. These findings can be associated with two different types of supramolecular stacking synthons observed in analyzed esters (Figure 6a). In the first one, the parallelly oriented molecules are substantially offset. The vertical distance ( $d$ ) between molecules is less than 3.4 Å, and a horizontal displacement ( $off$ ) is over 3 Å (Figure 6a, Table 4).

They are present in crystals where the C–H...O dimeric motif is observed apart from the pentafluoro derivative. In **pfphb** as well as in the **345fphb**, the antiparallel arrangement of molecules in stacking motifs is realized (Figure 6a). In the case of **345fphb**, the molecules are stacked around the screw axis with the offset close to zero. In **pfphb**, the interacting molecules are related by inversion centers with the offset of 1.8(1) and 2.1(1) Å. In these two esters, the highest dipole moment is observed (Table 2); hence, the dipole–antiparallel dipole interactions can be considered as decisive for molecular packing. It is noteworthy that the HOMO and LUMO orbitals' shapes (Figure 2) might suggest the charge-transfer nature of these antiparallel stacking interactions, but the value of the HOMO–LUMO energy gap estimated to be around 5 eV does not support this hypothesis.<sup>14</sup>

Further, the packing of molecules (Figure 7) may be discussed in terms of mutual dipole orientation. In Figure 8,

molecules are reduced to rods lying in accordance with the dipole moment vector's position and direction. Additionally, the dotted lines denote C–H...O hydrogen bonds leading to centrosymmetric dimers. Such a representation of molecular packing points to the structural similarity of **26fphb** and **246fphb**. It is also reflected in the comparable unit cell parameters and its symmetry. Hence, the crystals of **246fphb** and **26fphb** are isostructural. The dipole moments for these molecules optimized at the DFT/RB3LYP/6-311G(2df,p) level are relatively small and do not exceed 1D (Table 2, Figure 8). Even the change in dipole moment vector direction does not affect the crystal structure; thus the leading role of C–H...O directed centrosymmetric dimers is emphasized. In both crystals, the dimers are stacked in columns along the [100] direction. The neighboring columns are related by glide planes. They are joined by additional C–H...O and C–H...F interactions (Table 3).

The dimers are also dominant in the structure of **4fphb**. They assemble in stacks along the [010] direction, but in this case, the increase of dipole moment ( $\mu = 1.37$  D for optimized molecule at DFT/RB3LYP/6-311G(2df,p) level) causes their different arrangement when compared to **26fphb** and **246fphb** crystals. The adjacent columns are related here by  $2_1$  screw axes, and the weak dipole–dipole interactions between dimers might exist. Moreover, the C–H...F hydrogen bonds forming a head-to-tail C(11) chain motif along the [101] direction connect the stacked molecules (Figure 9). The resultant layers related by a screw axis are zipped by additional C–H...O interactions.

In the case of **pfphb** crystals, both the C–H...O dimers as well as antiparallel dipole arrangements are found. The last one can result from the relatively high molecular dipole moment ( $\mu = 2.18$  D obtained for optimized molecule at DFT/RB3LYP/6-311G(2df,p) level). The interactions of antiparallel dipoles occur between the neighboring centrosymmetric dimers related by the translation along [010] (Figure 8). A layered structure on the (001) plane is formed with the aid of dimeric C–H...F hydrogen bond motifs (Figure 9). Next, the neighboring layers related by a screw axis are joined by the C–H...F C(11) chain motif of a head-to-tail topology (Figure 9). It might be mentioned that, in the case of **pfphb**, the F...F separation of less than 2.9 Å is observed. The short contacts are visible on  $d_{\text{norm}}$  surfaces, but the resolved fingerprint plot (Figure S2 in the Supporting Information) does not show the characteristic sharp lines expected for halogen bonds.<sup>15,41</sup>

The molecule of **345fphb** exhibits the largest dipole moment ( $\mu = 3.12$  D, calculated at the DFT/RB3LYP/6-311G(2df,p) level), and the dipole–dipole interactions become dominant. Consequently, the dimers formed by C–H...O hydrogen bonds

are not observed. In this case, the antiparallel dipoles form stacks along the  $a$  axis. The adjacent columns are related by screw axis propagating along the [001] direction and by translation in the [010] direction (Figures 7 and 8). There are six columns surrounding the inner one, and the angle  $\theta$  between them (Table 4) is close to  $60^\circ$ . Thus, the pseudo hexagonal close-packed arrangement of stacks may be assumed (Figures 7 and 8). There are also the C–H $\cdots$ F hydrogen bonds between the stacks (Figure 9). The C(5) chain propagating along the [010] direction and showing a tail-to-tail topology is observed. This chain is supported by bifurcated C–H $\cdots$ F interactions joining the molecules related by the translation in a head-to-tail arrangement. The resulting ribbon has a rod group symmetry of  $p2_1^{32}$ .

## CONCLUSIONS

The detailed analysis of crystal structures of a series of fluorosubstituted phenylboronic catechol esters supported by Hirshfeld surface analysis and DFT calculations in the gas phase provide insights into the structural role of fluorine substituents. We have shown that, depending on the number and position of the fluorine substituents, the substantial differentiation of the molecular dipole moment is observed. We have also found that the presence of *ortho*-F substituents enhances the proton acceptor character of oxygen atoms, which favors the formation of the intermolecular C–H $\cdots$ O hydrogen bonds. Consequently, the packing of molecules is strongly affected by these effects, and two types of dominating supramolecular motifs can be distinguished: (i) the C–H $\cdots$ O hydrogen-bonded centrosymmetric dimer and (ii) the stacking columns directed by the antiparallel dipole–dipole interactions in the case of highly polar molecules. Additionally, we have concluded that, in crystals, the symmetry breaking of the idealized  $C_{2v}$  symmetry point group found for the DFT-optimized molecules may be the result of an asymmetry of the crystalline environment induced by the formation of intermolecular C–H $\cdots$ O and C–H $\cdots$ F hydrogen bonds.

## ASSOCIATED CONTENT

### Supporting Information

Tables S1 and S2 contain geometrical parameters for molecules derived on the basis of experimental and theoretical data. In Table S3, the values of vibrational frequencies for optimized molecules are collected. Figures S1 and S2 show full and resolved 2D-fingerprint plots for all characterized compounds in this paper, respectively. X-ray crystallographic information data (CIFs) are included at the end of the Supporting Information file. This material is available free of charge via the Internet at <http://pubs.acs.org>. Moreover, the CCDC 935154–935158 records contain the crystallographic data for this paper. These data can be obtained free of charge via <http://www.ccdc.cam.ac.uk/conts/retrieving.html> (or from the Cambridge Crystallographic Data Centre, 12, Union Road, Cambridge CB2 1EZ, U.K.; Fax: +44 1223 336033).

## AUTHOR INFORMATION

### Corresponding Author

\*E-mail: izabela@ch.pw.edu.pl. Fax: 48 22 628 2741. Tel: 48 22234 7272.

### Notes

The authors declare no competing financial interest.

## ACKNOWLEDGMENTS

The authors would like to thank Dr. J. Zachara for fruitful discussions and helpful comments considering the presented subject. The calculations reported in this work were partially performed at the Interdisciplinary Center for Mathematical and Computational Modeling of the University of Warsaw within grant No. G36-20. Financial support within grant No. NN 204127938 is kindly acknowledged. I.D.M. kindly acknowledges Warsaw University of Technology for the financial support.

## REFERENCES

- (1) See, for example: (a) Domenicano, A., Hargittai, I., Eds. *Strength from Weakness: Structural Consequences of Weak Interactions in Molecules, Supermolecules, and Crystals*; NATO Science Series; Kluwer Academic Publishers: Dordrecht, The Netherlands, 2002; Vol. 68.
- (b) Steed, J., Gale, P. A., Eds. *Supramolecular Chemistry: From Molecules to Nanomaterial*; John Wiley & Sons: Chichester, U.K., 2012.
- (2) Dunitz, J. D.; Gavezzotti, A. *Chem. Soc. Rev.* **2009**, *38*, 2622.
- (3) Desiraju, G. R. *J. Am. Chem. Soc.* **2013**, *135*, 9952.
- (4) (a) Desiraju, G. R. *Acc. Chem. Res.* **2002**, *35*, 565. (b) Desiraju, G. R. *Angew. Chem., Int. Ed.* **2011**, *50*, 52.
- (5) Gilli, G.; Gilli, P. *The Nature of the Hydrogen Bond: Outline of a Comprehensive Hydrogen Bond Theory*; Oxford University Press: Oxford, U.K., 2009.
- (6) (a) Desiraju, G. R.; Steiner, T. *The Weak Hydrogen Bond in Structural Chemistry and Biology*; Oxford University Press: New York, 1999. (b) Steiner, T. *Crystallogr. Rev.* **2003**, *9*, 177.
- (7) Desiraju, G. R. *Chem. Commun.* **2005**, 2995.
- (8) (a) Thalladi, V. R.; Weiss, H.-C.; Bläser, D.; Boese, R.; Nangia, A.; Desiraju, G. R. *J. Am. Chem. Soc.* **1998**, *120*, 8702. (b) Thakur, T. S.; Kirchner, M. T.; Bläser, D.; Boese, R.; Desiraju, G. R. *CrystEngComm* **2010**, *12*, 2079.
- (9) Chopra, D. *Cryst. Growth Des.* **2012**, *12*, 541.
- (10) Nishio, M. *Phys. Chem. Chem. Phys.* **2011**, *13*, 13873.
- (11) Melandri, S. *Phys. Chem. Chem. Phys.* **2011**, *13*, 13901.
- (12) Scheiner, S. *Phys. Chem. Chem. Phys.* **2011**, *13*, 13860.
- (13) Schneider, H.-J. *Chem. Sci.* **2012**, *3*, 1381.
- (14) (a) Salonen, L. M.; Ellermann, M.; Diederich, F. *Angew. Chem., Int. Ed.* **2011**, *50*, 4808. (b) Martinez, C. R.; Iverson, B. L. *Chem. Sci.* **2012**, *3*, 2191.
- (15) Metrangolo, P.; Resnati, G., Eds. *Halogen Bonding: Fundamentals and Applications, Structure and Bonding*; Springer-Verlag: Berlin, 2008; Vol. 126.
- (16) Lee, K.-M.; Chen, J. C. C.; Chen, H.-Y.; Lin, I. J. B. *Chem. Commun.* **2012**, *48*, 1242.
- (17) Thomas, S. P.; Pavan, M. S.; Guru Row, T. N. *Cryst. Growth Des.* **2012**, *12*, 6083.
- (18) Dunitz, J. D.; Taylor, R. *Chem.—Eur. J.* **1997**, *3*, 89.
- (19) (a) Pearson, R. G. *Chemical Hardness*; John Wiley-VCH: Weinheim, Germany, 1997. (b) Pearson, R. G. *J. Chem. Sci.* **2005**, *117*, 369.
- (20) Katrusiak, A.; Podsiadło, M.; Budzianowski, A. *Cryst. Growth Des.* **2010**, *10*, 3461.
- (21) Wheeler, S. E.; Houk, K. N. *J. Chem. Theory Comput.* **2009**, *5*, 2301.
- (22) Cozzi, F.; Bacchi, S.; Filippini, G.; Pilatic, T.; Gavezzotti, A. *CrystEngComm* **2009**, *11*, 1122.
- (23) (a) Collings, J. C.; Roscoe, K. P.; Thomas, R. L.; Batsanov, A. S.; Stimson, L. M.; Howard, J. A. K.; Marder, T. B. *New J. Chem.* **2001**, *25*, 1410. (b) Collings, J. C.; Roscoe, K. P.; Robins, E. G.; Batsanov, A. S.; Stimson, L. M.; Howard, J. A. K.; Clark, S. J.; Marder, T. B. *New J. Chem.* **2002**, *26*, 1740. (c) Cozzi, F.; Bacchi, S.; Filippini, G.; Pilati, T.; Gavezzotti, A. *Chem.—Eur. J.* **2007**, *13*, 7177.
- (24) Adamczyk-Woźniak, A.; Jakubczyk, M.; Sporzyński, A.; Żukowska, G. *Inorg. Chem. Commun.* **2011**, *14*, 1753.

- (25) Adamczyk-Woźniak, A.; Jakubczyk, M.; Jankowski, P.; Sporzyński, A.; Urbánski, P. M. *J. Phys. Org. Chem.* **2013**, *26*, 415.
- (26) (a) El-Kaderi, H. M.; Hunt, J. R.; Mendoza-Cortes, J. L.; Cote, A. P.; Taylor, R. E.; O'Keefe, M.; Yaghi, O. M. *Science* **2007**, *316*, 268. (b) Cote, A. P.; El-Kaderi, H. M.; Furukawa, H.; Hunt, J. R.; Yaghi, O. M. *J. Am. Chem. Soc.* **2007**, *129*, 12914.
- (27) Watanabe, T.; Miyaura, N.; Suzuki, A. *Synlett* **1992**, 207.
- (28) (a) Nishiyabu, R.; Kubo, Y.; James, T. D.; Fossey, J. S. *Chem. Commun.* **2011**, *47*, 1106. (b) Adamczyk-Woźniak, A. In *Phenylboronic Compounds as Molecular Recognition and Self-Assembling Agents: Application of Molecular Receptors*; Rybachenko, V. I., Ed.; Schidnyj wydawnyczyj dim: Donetsk, Ukraine, 2009; pp 9–24.
- (29) Jańczyk, M.; Adamczyk-Woźniak, A.; Sporzyński, A.; Wróblewski, W. *Anal. Chim. Acta* **2012**, *733*, 71.
- (30) (a) Sarma, R.; Baruah, J. B. *J. Mol. Struct.* **2009**, *920*, 350. (b) Sarma, R.; Bhattacharyya, P. K.; Baruah, J. B. *Comput. Theor. Chem.* **2011**, *963*, 141.
- (31) Cyrański, M. K.; Klementowska, P.; Rydzewska, A.; Serwatowski, J.; Sporzyński, A.; Stępień, D. K. *CrystEngComm* **2012**, *14*, 6282.
- (32) Durka, K.; Jarzembska, K. N.; Kamiński, R.; Luliński, S.; Serwatowski, J.; Woźniak, K. *Cryst. Growth Des.* **2012**, *12*, 3720.
- (33) *CrysAlisPro*, Version 1.171.35.7; Agilent Technologies: Santa Clara, CA, 2011; (release 14-02-2011 CrysAlis171.NET).
- (34) Dolomanov, O. V.; Bourhis, L. J.; Gildea, R. J.; Howard, J. A. K.; Puschmann, H. *J. Appl. Crystallogr.* **2009**, *42*, 339.
- (35) Sheldrick, G. M. *Acta Crystallogr., Sect. A* **2008**, *64*, 112.
- (36) (a) Flack, H. D.; Bernardinelli, G. *Acta Crystallogr., Sect. A* **1999**, *55*, 908. (b) Flack, H. D.; Bernardinelli, G. *J. Appl. Crystallogr.* **2000**, *33*, 1143.
- (37) Spek, L. *J. Appl. Crystallogr.* **2003**, *36*, 7.
- (38) Brandenburg, K. *Diamond: Crystal and Molecular Structure Visualization*, Version 3.2i; Crystal Impact GbR: Bonn, Germany, 2012.
- (39) Farrugia, L. *J. Appl. Crystallogr.* **1999**, *32*, 837.
- (40) Frisch, M. J.; Trucks, G. W.; Schlegel, H. B.; Scuseria, G. E.; Robb, M. A.; Cheeseman, J. R.; Scalmani, G.; Barone, V.; Mennucci, B.; Petersson, G. A.; Nakatsuji, H.; Caricato, M.; Li, X.; Hratchian, H. P.; Izmaylov, A. F.; Bloino, J.; Zheng, G.; Sonnenberg, J. L.; Hada, M.; Ehara, M.; Toyota, K.; Fukuda, R.; Hasegawa, J.; Ishida, M.; Nakajima, T.; Honda, Y.; Kitao, O.; Nakai, H.; Vreven, T.; Montgomery, J. A., Jr.; Peralta, J. E.; Ogliaro, F.; Bearpark, M.; Heyd, J. J.; Brothers, E.; Kudin, K. N.; Staroverov, V. N.; Kobayashi, R.; Normand, J.; Raghavachari, K.; Rendell, A.; Burant, J. C.; Iyengar, S. S.; Tomasi, J.; Cossi, M.; Rega, N.; Millam, J. M.; Klene, M.; Knox, J. E.; Cross, J. B.; Bakken, V.; Adamo, C.; Jaramillo, J.; Gomperts, R.; Stratmann, R. E.; Yazeyev, O.; Austin, A. J.; Cammi, R.; Pomelli, C.; Ochterski, J. W.; Martin, R. L.; Morokuma, K.; Zakrzewski, V. G.; Voth, G. A.; Salvador, P.; Dannenberg, J. J.; Dapprich, S.; Daniels, A. D.; Farkas, Ö.; Foresman, J. B.; Ortiz, J. V.; Cioslowski, J.; Fox, D. J. *Gaussian 09*, Revision A.1; Gaussian, Inc.: Wallingford, CT, 2009.
- (41) Spackman, M. A.; Jayatilaka, D. *CrystEngComm* **2009**, *11*, 19 and references therein.
- (42) McKinnon, J. J.; Jayatilaka, D.; Spackman, M. A. *Chem. Commun.* **2007**, 3814 and references therein.
- (43) Wolff, S. K.; Grimwood, D. J.; McKinnon, J. J.; Jayatilaka, D.; Spackman, M. A. *CrystalExplorer*, Version 2.1; University of Western Australia: Crawley, Australia, 2007.
- (44) Allen, F. H. *Acta Crystallogr., Sect. B* **2002**, *58*, 380.
- (45) Neu, R. C.; Ouyang, E. Y.; Geier, S. J.; Zhao, X.; Ramos, A.; Stephan, D. W. *Dalton Trans.* **2010**, *39*, 4285.
- (46) Oh, S.-W.; Weiss, J. W. E.; Kerneghan, P. A.; Korobkov, I.; Maly, K. E.; Bryce, D. L. *Magn. Reson. Chem.* **2012**, *50*, 388.
- (47) Zettler, F.; Hausen, H. D.; Hess, H. *Acta Crystallogr., Sect. B* **1974**, *30*, 1876.
- (48) Zabrodsky, H.; Peleg, S.; Avnir, D. *J. Am. Chem. Soc.* **1993**, *115*, 8278.
- (49) Wunderlicht, H.; Mootz, D. *Acta Crystallogr., Sect. B* **1971**, *27*, 1684.
- (50) Niu, W.; Smith, M. D.; Lavigne, J. *J. Cryst. Growth Des.* **2006**, *6*, 127.
- (51) (a) Etter, M. C. *Acc. Chem. Res.* **1990**, *23*, 120. (b) Etter, M. C.; MacDonald, J. C.; Bernstein, J. *Acta Crystallogr., Sect. B* **1990**, *46*, 256.
- (52) Kopsky, V., Litvin, D. B., Eds. *International Tables for Crystallography: Subperiodic Groups*; Kluwer Academic Publishers: Dordrecht, The Netherlands, 2002; Vol. E.